Publ. Astron. Soc. Aust., 1999, 16, 89–94

Constraints on Cold HI in the Halo of NGC 3079 from Absorption Measurements of Q0957+561

Judith A. Irwin[1,2], Lawrence M. Widrow[1] and Jayanne English[3]

[1] Queen's University, Kingston, Ontario K7L 3N6, Canada
irwin@astro.queensu.ca, widrow@astro.queensu.ca

[2] National Centre for Radio Astrophysics, Pune University Campus, Post Bag 3, Pune 411 007, India

[3] Space Telescope Science Institute, 3700 San Martin Drive, Baltimore, MD 21218, USA
jenglish@stsci.edu

Received 1998 November 17, accepted 1999 February 8

Abstract: We perform the first observational test of dark matter in the form of cold (3 K) fractal clouds, as described by Pfenniger et al. (1994) and Pfenniger & Combes (1994). This is accomplished by probing for HI absorption in the halo of NGC 3079 against the background quasar, Q 0957+561, which is separated from the centre of NGC 3079 by 64 kpc, in projection. No absorption is detected to a limit of $3\,\Delta T_{\rm b}/(-T_{\rm c}) = 0{\cdot}01$. We have considered models for HI + H_2 clouds characterised by the cloud radius and fractal dimension. Using the upper limit on absorption, we have ruled out a limited but interesting region of this parameter space. The observations do not rule out the possibility that all the dark matter could be hidden in the form of cold fractal clouds. By contrast, if the gas is diffuse with unity filling factors, then HI cannot constitute more than $\sim 10^{-5}$, by mass, of the galaxy's dark matter.

Keywords: dark matter — galaxies: halos — galaxies: individual (NGC 3079) — ISM: structure

1 Introduction

Primordial nucleosynthesis calculations, together with estimates for the density of luminous matter, indicate that at least some baryonic dark matter is present in the Universe. Baryonic matter has received renewed attention of late (see Carr 1994), especially in the light of recent reports of gravitational lensing events, presumably from massive compact halo objects around the Milky Way. Other possibilities for baryonic dark matter have also been proposed. For example, several authors have investigated the possibility that this matter could be in the form of gas (e.g. Henriksen 1991; Henriksen & Widrow 1995; Pfenniger, Combes & Martinet 1994; Pfenniger & Combes 1994).

1.1 Dark Matter as Cold Fractal Clouds

Recently, Pfenniger, Combes & Martinet (1994) and Pfenniger & Combes (1994) (hereafter PCM and PC respectively) proposed a new dark matter candidate: cold primordial H_2 gas in a fractal structure. The gas resides in an extended disk or halo where the only source of heating is the 3 K background. PCM contend that the slow accretion of gas toward the visible disk solves the 'gas consumption problem' (i.e. that the timescale for gas consumption, as implied by current star formation rates, is shorter than the age of the galaxy) as well as the 'disk–halo conspiracy' (i.e. flat rotation curves through the transition region from disk to halo-dominated rotation). The motivation for a fractal-like distribution comes, in part, from observations of the ISM where both atomic and molecular hydrogen clouds exhibit hierarchical structure over a wide range of scales (see e.g. Diamond et al. 1989; Vogelaar & Wakker 1994 Elmegreen & Falgarone 1996).

In this paper, we describe our attempt to detect cold HI gas by searching for absorption features against a background continuum source. At the cold temperatures envisaged by PCM and PC, neither HI nor H_2 can be seen in emission. Moreover, if the gas is primordial, it would not be traceable via other molecules such as CO. HI absorption may represent a unique opportunity to constrain, through observations, the PCM and PC hypothesis, provided not all of the hydrogen is converted to molecular form (see below).

1.2 Fractal Cloud Parameters

In the PCM and PC scenario, the hydrogen cloud complexes are built out of elementary 'cloudlets' ('clumpuscules' by PC). The size of these objects

 1323-3580/99/010089$05.00

(determined by setting the free-fall timescale equal to the Kelvin–Helmholtz timescale and assuming virialisation) sets a minimum scale below which the gas distribution is no longer described by a fractal. For $T = 3\,\mathrm{K}$ neutral gas, these cloudlets are characterised by the following parameters: mass, $M_* = 0{\cdot}8\text{–}9{\cdot}2 \times 10^{-3}\ M_\odot$; radius, $R_* = 23\text{–}150$ AU; number density, $n_* = 0{\cdot}25 - 6 \times 10^9\ \mathrm{cm}^{-3}$; column density, $N_* = 0{\cdot}73 - 2{\cdot}7 \times 10^{24}\ \mathrm{cm}^{-2}$; and velocity dispersion, $v_* = 0{\cdot}10 - 0{\cdot}14\ \mathrm{km\ s}^{-1}$. The range is due to departures from spherical symmetry and black body radiation (PC's factor f), as well as differences in mean molecular weight μ between pure HI + He and pure H_2 + He.

A key unknown is the atomic to molecular hydrogen ratio. At the densities found in the cloudlets, the three-body reactions $H + H + H \rightarrow H + H_2$ and $H + H + H_2 \rightarrow H_2 + H_2$ may be important in converting atomic hydrogen into H_2 (see Palla, Salpeter & Stahler 1983). Let us assume that at the time when the fractal structure develops, t_0, all of the hydrogen gas is in atomic form, with number density $n_{\mathrm{HI}}(t_0)$. At late times t, the number density will be given roughly by $n_{\mathrm{HI}}(t) = [\mathcal{R}(T)\,(t - t_0)\,n_{\mathrm{HI}}(t_0)]^{-1}$ where $\mathcal{R}(T)$ is the rate constant for the reaction $H + H + H_2 \rightarrow H_2 + H_2$. Here $\mathcal{R}(T)$ has been determined only for much higher temperatures ($\sim$ 3000 K). Extrapolating over 3 orders of magnitude to 3 K gives $\mathcal{R}(T) = 2{\cdot}3 \times 10^{-30}\,\mathrm{cm}^6\ \mathrm{s}^{-1}\ (3K/T)$. Taking $t - t_0 \sim 10\,\mathrm{Gyr}$, then $n(\mathrm{HI})_* \sim 550\text{–}5500\ \mathrm{cm}^{-3}$. This corresponds to HI optical depths of 0·5 to 13. Rawlings (1988) quoted a reaction rate 2 orders of magnitude lower which increases the HI fraction and optical depth proportionately. We will therefore consider $n(\mathrm{HI})_*/n_*$ to be a free parameter, f_{HI}, with HI and H_2 coexisting throughout the cloudlets. In this initial treatment, we consider optically thick HI, assume no departures from spherical symmetry (PC's parameter, $f = 1$) and let $\mu = 2{\cdot}3$. The cloudlet parameters are then $M_* = 0{\cdot}8 \times 10^{-3}\ M_\odot$, $R_* = 23$ AU, $n_* = 6 \times 10^9\ \mathrm{cm}^{-3}$, $N_* = 2{\cdot}7 \times 10^{24}\ \mathrm{cm}^{-2}$ and $v_* = 0{\cdot}10\ \mathrm{km\ s}^{-1}$.

The cloudlets combine in a fractal structure to form clouds (denoted with subscript c below) which have parameters related to the parameters of the cloudlets via

$$M_{\mathrm{c}} = \mathcal{N}_{\mathrm{c}} M_* = \left(\frac{R_{\mathrm{c}}}{R_*}\right)^D M_*, \quad n_{\mathrm{c}} = \left(\frac{R_{\mathrm{c}}}{R_*}\right)^{D-3} n_*,$$
$$N(\mathrm{HI})_{\mathrm{c}} = \left(\frac{R_{\mathrm{c}}}{R_*}\right)^{D-2} f_{\mathrm{HI}}\, N_*, \quad v_{\mathrm{c}} = \left(\frac{R_{\mathrm{c}}}{R_*}\right)^{(D-1)/2} v_*\,. \tag{1}$$

Here $\mathcal{N}_{\mathrm{c}}$ is the number of cloudlets in a cloud, the quantity, R_{c}/R_* is the scale over which fractal structure exists and D is the fractal dimension. We expect $D \lesssim 2$ since for $D > 2$, collisions tend to dissipate the cloud (PC). The value $D = 2$ corresponds to an area covering factor of unity and we therefore assume that cloudlets within a single cloud do not shadow one another. For simplicity, we also extend the no-shadowing assumption to velocity space and to cloud/cloud shadowing. For clouds of equivalent mass, a lower value of D implies that the cloud will be larger and less dense.

1.3 The NGC 3079–Q 0957 + 561 Pair

A fortuitous alignment of the extension of the major axis of the galaxy, NGC 3079, with the background quasar, Q0957+561 (Figure 1, left) has provided the opportunity to search for cold gas in an extended halo or an extended disk around the foreground galaxy. NGC 3079 ($D = 15{\cdot}6$ Mpc; $H_0 = 75\ \mathrm{km\ s}^{-1}\ \mathrm{Mpc}^{-1}$) has been mapped in HI by Irwin & Seaquist (1991). The outermost point at which emission is observed is denoted by a small star in Figure 1. Q0957+561 is a gravitationally lensed system (Walsh, Carswell & Weymann 1979) at a redshift of $z = 1{\cdot}4$ (see Schmidt & Wambsganss 1998 and references therein). The projected separation between the centre of NGC 3079 and Q0957 + 561 is 64·1 kpc at the distance of NGC 3079. A dark matter halo may extend between 100 and 200 kpc in radius (see Ashman 1992). For our purposes, we consider the lensed quasar to be simply a source of background radio continuum emission.

2 Observations

HI observations were carried out on 1997 January 3 in the A configuration of the Very Large Array (VLA)* using flux calibrators, J1331+305 (3C286) and J0137+331 (3C48), and phase calibrator, J0957+553. Appropriate uv restrictions were applied during calibration. The field centre was placed 13 arcseconds south of the quasar to avoid baseline-dependent map errors which tend to show up at the field centre and, for highest sensitivity, the 4IF mode was used.

The central observing velocity was set to 974 km s^{-1}, which is between the velocities expected for a flat rotation curve and a Keplerian fall-off for NGC 3079, and encompasses both possibilities with a total bandwidth of 163·4 km s^{-1}. The band contained 63 spectral channels which, with on-line Hanning smoothing, gave a final channel width (= spectral resolution) of 2·59 km s^{-1}.

The primary flux density calibrators were also used as bandpass calibrators and were observed four times during the 10 hours of observations.

*The National Radio Astronomy Observatory is a facility of the National Science Foundation operated under cooperative agreement by Associated Universities, Inc.

https://doi.org/10.1071/AS99089 Published online by Cambridge University Press

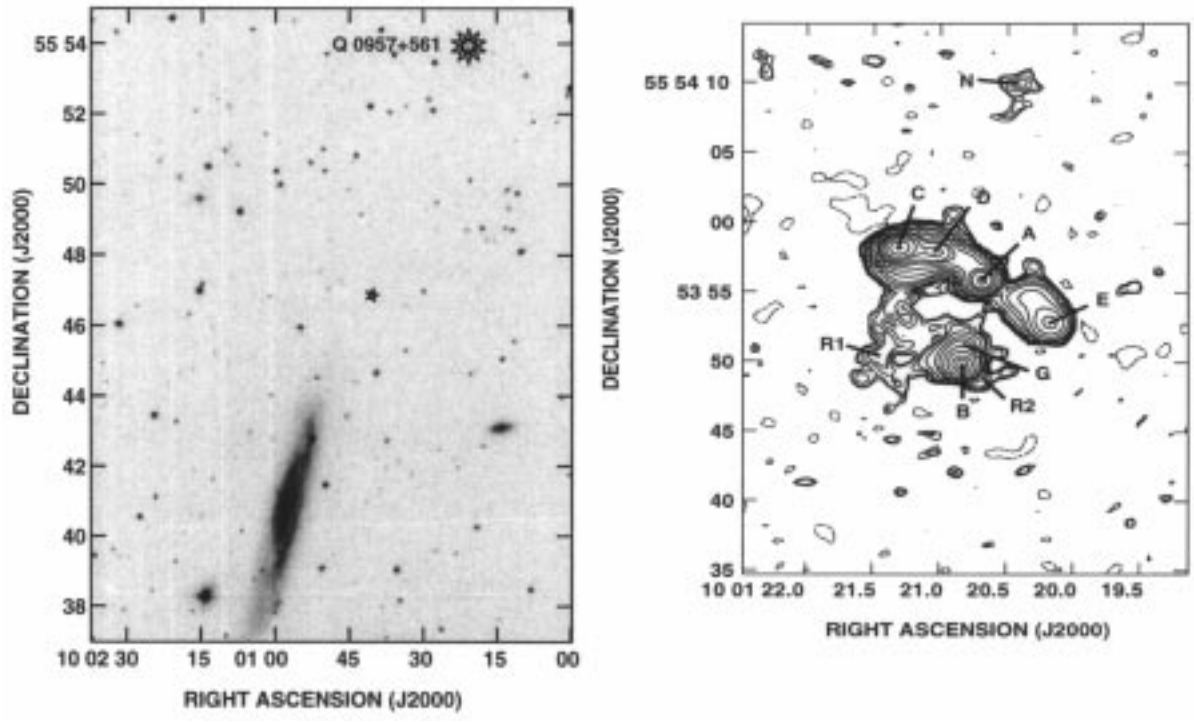

Figure 1—*Left:* Optical image of NGC 3079, showing the position of the background quasar, Q 0957 + 561 (large star). The small star denotes the outermost point at which HI is observed in emission around NGC 3079 (Irwin & Seaquist 1991). *Right:* Continuum image of Q 0957+561, labelled according to Greenfield, Roberts & Burke (1985) and Avruch et al. (1997). Contours are at $-0{\cdot}26$, $0{\cdot}26$ (2σ), $0{\cdot}3$, $0{\cdot}4$, $0{\cdot}5$, $0{\cdot}8$, $1{\cdot}5$, $2{\cdot}5$, 5, 10, 20, 30, 50, 75, 120 and 170 mJy beam^{-1} and the beam size is $1{\cdot}31'' \times 1{\cdot}15''$ at position angle, $-87{\cdot}31°$.

The calibration observation closest in time to the source observation was applied. Examination of the average bandpass for each time showed that the maximum temporal change in the bandpass over the four scans was of order $0{\cdot}2\%$.

UV data for each channel were Fourier transformed and cleaned using uniform weighting to create a total emission (RA–DEC–Velocity) cube. A continuum image was also made by averaging together the uv data for all low-noise channels before Fourier transformation. The data were phase-only and then phase+amplitude self-calibrated until no improvement in rms resulted.

A continuum-subtracted cube was made by subtracting a linear fit to the visibilities from each low-noise total emission channel. The resulting rms noise in the continuum-subtracted maps is $0{\cdot}58 \pm 0{\cdot}01$ mJy beam^{-1}, where the error represents the 1σ variation over all channels. Channel-to-channel variations due to the bandpass calibration are smaller than this. The spectral dynamic range, i.e. the ratio of peak continuum intensity to rms noise in the channel maps is $\sim 300/1$.

3 Results

The continuum map is shown in Figure 1 (right), with components labelled according to Greenfield, Roberts & Burke (1985) and Avruch et al. (1997). The lensing galaxy is associated with radio source G, seen as a northern extension to component B. There are 28 beams across this background emission at levels $> 10 \times$ the rms noise, i.e. we have 28 independent probes of HI absorption per channel.

The HI continuum-subtracted cube was inspected for signs of emission or absorption features. No HI features were detected above $\sim 3 \times$ the rms noise per channel. The same conclusion is reached if a continuum map is subtracted from a more restricted range of velocity channels, if the naturally weighted maps are instead examined, or if the continuum-subtracted cube is smoothed over systematically varying velocity or spatial ranges.

4 Constraints on Fractal HI in a Dark Matter Halo

4.1 Density of Dark Matter at Position of Q 0957 + 561

We model the dark matter distribution in the galaxy as an isothermal spheroid

$$\bar{\rho} = \frac{\lambda(q) V_c^2}{4\pi G} \frac{1}{R^2 + z^2/q^2}\,, \qquad (2)$$

where V_c is the circular rotation speed, R is the galactocentric radius in the plane of the disk, z is the coordinate perpendicular to the plane ($r^2 = R^2 + z^2$), q is the flattening parameter ($q < 1$ for an oblate halo), $\lambda(q)$ is a geometric factor equal to 1 for $q = 1$ and rising to $6{\cdot}8$ for $q = 0{\cdot}1$. For $V_c = 215$ km s^{-1}

https://doi.org/10.1071/AS99089 Published online by Cambridge University Press

(Irwin & Seaquist 1991), $R = 64$ kpc, $z = 0$, and assuming that the r^{-2} profile extends out well beyond 64 kpc, the mean surface density at the position of the quasar is then

$$\overline{N} = \begin{cases} 3{\cdot}3 \times 10^{21} \ \mathrm{cm}^{-2} & \text{for } q = 1 \\ 2{\cdot}2 \times 10^{22} \ \mathrm{cm}^{-2} & \text{for } q = 0{\cdot}1 \end{cases} . \quad (3)$$

4.2 The Observational Parameters

For HI clouds in front of a uniform background continuum source, the brightness temperature $T_{\rm B}$ observed in a given beam and velocity channel is given by

$$T_{\rm B} = [T_{\rm c}\ {\rm e}^{-\tau} + T_{\rm s}(1 - {\rm e}^{-\tau})] + \mathcal{N}\, f_{\rm v}\ f_{\rm b} + T_{\rm c}(1 - \mathcal{N}\ f_{\rm v}\ f_{\rm b}), \quad (4)$$

where $T_{\rm c}$ is the brightness temperature of the background continuum, $T_{\rm s}$, τ are the spin temperature and optical depth, respectively, of the gas, $f_{\rm b}$, $f_{\rm v}$ are the beam area and velocity filling factors, respectively, for a single cloud, and $\mathcal{N}$ is the number of clouds in the beam/velocity resolution element. Thus, the quantity $\mathcal{N} f_{\rm v} f_{\rm b}$ is the filling factor for a resolution element. Since only a part of a cloud may fall within a beam, $\mathcal{N}$ can be less than 1. Alternatively, $\mathcal{N} < 1$ can be thought of as the probability of finding a cloud in a given beam.

After continuum-subtraction, we have

$$\Delta T_{\rm B} = (T_{\rm s} - T_{\rm c})(1 - e^{-\tau})\, \mathcal{N}\, f_{\rm v}\, f_{\rm b}\,. \quad (5)$$

This is the measured quantity in the continuum-subtracted cubes, in temperature units. If $T_{\rm c} \gg T_{\rm s}$ (which is the case for almost all lines of sight to the background continuum, Figure 1 right), then a ratio map can be formed by computing $\Delta T_{\rm B}/(-T_{\rm c})$ for each line of sight to the background continuum for any channel. In the optically thick and optically thin limits, this ratio is

$$\frac{\Delta T_{\rm B}}{-T_{\rm c}} = \begin{cases} \mathcal{N}\, f_{\rm v}\ f_{\rm b} & \text{for } \tau > 1 \text{ (fractal clouds)} \\ \tau\ \mathcal{N}\, f_{\rm v}\ f_{\rm b} & \text{for } \tau < 1 \text{ (diffuse gas)}\,. \end{cases} \quad (6)$$

We have only an upper limit to $\Delta T_{\rm B}$ which we take to be 3 × the rms map noise, identical for each channel. Thus the ratio map is the same for any channel and has the appearance of the reciprocal of the continuum map. This ratio map would be a map of optical depth under the more common assumptions of unity filling factors and optically thin gas.

The minimum value of the computed ratio map is 0·01. Thus, if the gas consists of fractal clouds, our strongest constraint is that $\mathcal{N} f_{\rm v} f_{\rm b} \leq 0{\cdot}01$ (*Condition 1*). If such fractal clouds exist, then they would not be detected if the filling factor in a resolution element is less than this observationally determined limit. This could mean either that there were clouds in the beam/channel ($\mathcal{N} \geq 1$) but their filling factors were too low for detection, or that there were no clouds or too small a fraction of a cloud within the beam/channel for detection. The second possibility, we represent as $\mathcal{N} < 0{\cdot}15$. This is derived by requiring that the probability of there being a cloud in at least one of the 28 beams be $> 99\%$. (Note that this also assumes that the probability of detecting a cloud is equivalent in each of the 28 beams. In fact, this probability depends on the varying strength of the background continuum and thus this quantity may be revised.) We can now express the filling factors in terms of fractal parameters. The velocity and beam filling factors are dealt with separately since there are different conditions under which these two filling factors become unity.

The velocity filling factor in a channel of width $\Delta v_{\rm ch}$ is the number of clouds $\mathcal{N}$ times the channel filling factor for a single cloud $f_{\rm v}$, i.e.

$$\mathcal{N}\ f_{\rm v} = \min\left\{\mathcal{N}\ \left(\frac{v_{\rm c}}{\Delta v_{\rm ch}}\right), 1\right\} = \min\left\{\mathcal{N}\ \left(\frac{R_{\rm c}}{R_*}\right)^{(D-1)/2}\left(\frac{v_*}{\Delta v_{\rm ch}}\right), 1\right\}, \quad (8)$$

where equation (8) has made use of equation (1). The right term in the braces indicates the case in which the cloud or clouds 'fill' the velocity channel.

The area filling factor in a beam of radius $R_{\rm b}$ is the number of clouds $\mathcal{N}$ times the beam filling factor for a single cloud $f_{\rm b}$, i.e.

$$\mathcal{N}\ f_{\rm b} = \min\left\{\mathcal{N}\ \left(\frac{R_{\rm c}}{R_*}\right)^{(D-2)}\left(\frac{R_{\rm c}}{R_{\rm b}}\right)^{2}, \left(\frac{R_{\rm b}}{R_*}\right)^{(D-2)}\right\} \quad (9)$$

$$= \min\left\{\mathcal{N}\ \left(\frac{R_{\rm c}}{R_*}\right)^{D}\left(\frac{R_*}{R_{\rm b}}\right)^{2}, \left(\frac{R_{\rm b}}{R_*}\right)^{(D-2)}\right\}, \quad (10)$$

where we assume $D < 2$. The term $(R_{\rm c}/R_*)^{(D-2)}$ is the area filling factor for cloudlets in a single fractal cloud and the right term in the braces indicates the case in which the cloud or clouds fill the area of the beam (except for the filling factor of the cloudlets).

These two expressions, which assume no-overlap of clouds or cloudlets, along with Condition 1 allow us to place constraints on the fractal parameters, $R_{\rm c}$ and D.

4.3 Results for Fractal Clouds

Figure 2 (left) shows the results, assuming that the clouds fill the velocity channel ($\mathcal{N} f_{\rm v} = 1$), which puts

https://doi.org/10.1071/AS99089 Published online by Cambridge University Press

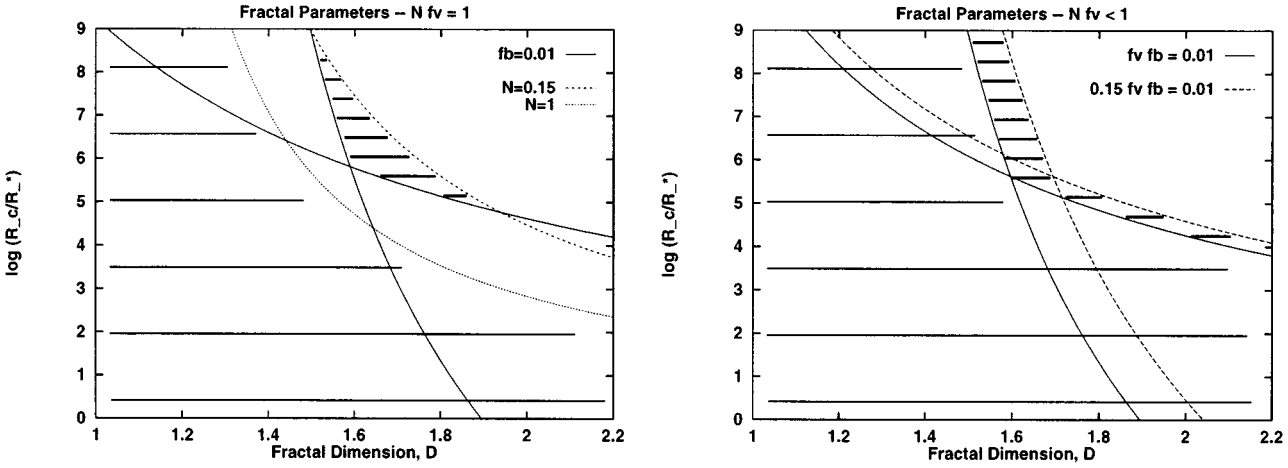

Figure 2—*Left:* Fractal parameters for the case in which the clouds fill velocity space. The solid curves denote the observational limit when the clouds do not fill the beam (more horizontal curve) and when they do (more vertical curve). The dashed curve represents $\mathcal{N} = 0{\cdot}15$ above which a cloud would not be in the beam and the dotted curve represents $\mathcal{N} = 1$. *Right:* Fractal parameters for the case in which the clouds do not fill velocity space. The solid curves denote the observational limit (as at left) for the case, $\mathcal{N} = 1$, and the dotted curves represent $\mathcal{N} = 0{\cdot}15$.

a limit on the number of clouds in a beam/velocity resolution element, i.e. $\mathcal{N} = 1/f_{\rm v}$. The two solid curves denote Condition 1, i.e. $f_{\rm b} = 0{\cdot}01$, with the more horizontal curve corresponding to the case in which the clouds do not fill the beam and the more vertical curve corresponding to the case in which they do. The number of clouds in the resolution element varies along the solid curve. If fractal clouds exist and occur within a beam, they would not have been detected if they have parameters which fall below these curves. The dashed line indicates the condition $\mathcal{N} = 0{\cdot}15$. Above this curve, fractal clouds would not have been detected because there is a low probability that the cloud is within the beam. Thus, we can rule out parameter space which falls between these curves; this region is denoted by the bold horizontal lines in the figure.

In addition, the velocity resolution is quite fine ($2{\cdot}6$ km s^{-1}). Suppose that there are two clouds within the beam, i.e. separated by $\lesssim 95$ pc. For these clouds to be within the same beam/channel element, they must be separated in velocity by $<2{\cdot}6$ km s^{-1}. Yet observed velocity dispersions in disk gas are of order 10 km s^{-1}, independent of radius, and may be higher in an extended dark matter disk, given the requirement of disk stability (see the discussion in PCM). If this is the case, then it is unlikely that these clouds would be separated in velocity by less than $2{\cdot}6$ km s^{-1} which suggests that $\mathcal{N} \leq 1$. Under these circumstances, we can also rule out the region of parameter space marked by the thin horizontal lines under the $\mathcal{N} = 1$ (dotted) curve.

Figure 2 (right) shows the results for the case in which the clouds do not fill the velocity channel ($\mathcal{N} f_{\rm v} < 1$). The solid curves denote the case $\mathcal{N} = 1$, and the dotted curves denote $\mathcal{N} = 0{\cdot}15$. Thus, we can rule out parameter space between these curves, shown by horizontal bold lines. Again, if $\mathcal{N} \leq 1$, then the region marked by thin horizontal lines can also be ruled out.

We can now compute the mean column density in a beam, $\overline{N({\rm HI})} = \mathcal{N}(R_{\rm c}/R_{\rm b})^2 N({\rm HI})_{\rm c}$, for fractal parameters which fall below our observational limit and compare this to the theoretically expected value for a dark matter halo (equation 3). The results indicate that it is possible to 'hide' all the dark matter in fractal clouds. For example (Figure 2, left), $D = 1{\cdot}6$ and $\log(R_{\rm c}/R_*) = 5{\cdot}7$ are (just) below the observational limit. These parameters yield a value of $\overline{N({\rm HI})} = f_{\rm H} \times 1{\cdot}3 \times 10^{22}$ cm^{-2}. Then the mean column density of HI + H_2 gas in fractal clouds is $\overline{N_{\rm f}} = 1{\cdot}3 \times 10^{22}$ cm^{-2} which (cf. equation 3) implies that virtually all the dark matter could be hidden in such clouds.

4.4 Results for Diffuse HI

It is interesting to contrast the above results with what would be obtained if we make the more common assumptions that the gas is optically thin and the filling factors are all 1. In this case, the observational limit can be written as $\tau \leq 0{\cdot}01$ (equation 6) which gives $\overline{N({\rm HI})} \leq 4{\cdot}7 \times 10^{16} T_{\rm s}$ cm^{-2}, illustrating the high sensitivity of these observations. For $T_{\rm s} = 3$ K, a comparison with the theoretical value for spherical and flattened halos (equation 3) implies that HI cannot constitute more than $\sim 10^{-5}$ of the dark matter, if it is in the form of cold diffuse gas.

5 Conclusions

We have searched for HI absorption in the halo of NGC 3079 against the background quasar Q $0957+561$ in the first observational test of dark matter as cold fractal clouds. No absorption is detected to a limit

https://doi.org/10.1071/AS99089 Published online by Cambridge University Press

of $3\,\Delta T_{\rm b}/(-T_{\rm c}) = 0{\cdot}01$. Assuming that HI exists in some proportion with H_2 in fractal clouds at 3 K, we can rule out limited regions of parameter space, i.e. the fractal dimension D, and the scale over which fractal structure exists $R_{\rm c}/R_{*}$, as indicated in Figure 2. Given the fine velocity resolution of the observations, it is reasonable to assume that multiple clouds in a beam/resolution element are unlikely, which places additional constraints on D and $R_{\rm c}/R_{*}$. However, we cannot rule out the possibility that all the dark matter could be hidden in cold fractal clouds, since regions of parameter space which allow this possibility fall below our observational threshold. By contrast, if HI is in the form of cold, diffuse gas with unity filling factors, then it cannot constitute more than $\sim 10^{-5}$, by mass, of the dark matter.

Acknowledgments

We thank R. N. Henriksen for informative discussions and Mark Walker for important and useful criticisms. This work was supported by a grant from the Natural Sciences and Engineering Research Council of Canada.

References

Ashman, K. 1992, PASP, 104, 1109
Avruch, I. M., Cohen, A. S., Lehár, J., Conner, S. R., Haarsma, D. B., & Burke, B. F. 1997, ApJ, 488, L121
Carr, B. 1994, ARAA, 32, 531
Diamond, P. J., et al. 1989, ApJ, 347, 302
Elmegreen, B. G., & Falgarone, E. 1996, ApJ, 471, 816
Greenfield, P. E., Roberts, D. H., & Burke, B. F. 1985, ApJ, 293, 370
Henriksen, R. N. 1991, ApJ, 377, 500
Henriksen, R. N., & Widrow, L. M. 1995, ApJ, 441, 70
Irwin, J. A., & Seaquist, E. R. 1991, ApJ, 371, 111
Palla, F., Salpeter, E. E., & Stahler, S. W. 1983, ApJ, 271, 632
Pfenniger, D., & Combes, F. 1994, A&A, 285, 94 (PC)
Pfenniger, D., Combes, F., & Martinet, L. 1994, A&A, 285, 79 (PCM)
Rawlings, J. M. C. 1988, MNRAS, 232, 507
Schmidt, R., & Wambsganss, J. 1998, A&A, 335, 379
Vogelaar, M. G. R., & Wakker, B. P. 1994, A&A, 291, 557
Walsh, D., Carswell, R. F., & Weymann, R. J. 1979, Nature, 179, 381

https://doi.org/10.1071/AS99089 Published online by Cambridge University Press